INSTITUTE OF PHYSICS PUBLISHING PLASMA PHYSICS AND CONTROLLED FUSION

Plasma Phys. Control. Fusion **45** (2003) 1989–1999 PII: S0741-3335(03)68168-6

Experimental study and two-dimensional modelling of the plasma dynamics of magnetically driven shock waves in a coaxial tube

C Moreno[1], F Casanova[2], G Correa[2] and A Clausse[2]

[1] Instituto de Física del Plasma—PLADEMA, Departamento de Física, Facultad de Ciencias Exactas y Naturales, Universidad de Buenos Aires, 1428 Buenos Aires, Argentina
[2] PLADEMA, CNEA-CONICET and Universidad Nacional del Centro, 7000 Tandil, Argentina

Received 20 August 2003
Published 28 October 2003
Online at stacks.iop.org/PPCF/45/1989

Abstract

Plasma shocks can be magnetically driven during high current discharges in low-pressure gases, induced by an external electric circuit. Radial currents between two coaxial electrodes can be accelerated to velocities of the order of $10\,\mathrm{cm}\,\mu\mathrm{s}^{-1}$, thus being an effective method to transform potential energy in kinetic energy. A series of experiments were conducted using a low energy plasma focus device to measure the dynamics of plasma shocks in coaxial tubes. The radial position of the current sheath near the closed end of the electrodes was determined by means of a magnetic probe. The pinching time at the open end of the electrodes was measured using a Rogowski coil. Both, the movement and shaping of the plasma sheath were modelled by means of finite elements. The sheath was represented by coupled conical segments carrying current, mass, internal energy and momentum. The Lorentz force accelerates each element in its normal direction, which leads to the continuous reshaping of the sheath. The numerical results are compared against the experimental data showing good agreement.

Nomenclature

A_i	surface area associated with the ith segment
B	magnetic field strength
C	capacity
J	current density
e	specific internal energy
e_I	ionization energy, $6.5 \times 10^8\,\mathrm{J\,kg^{-1}}$ for deuterium
I	current
l_i	length of the ith segment

0741-3335/03/121989+11$30.00

l_i^{new}	corrected length of the ith reshaped segment
L_{ext}	external inductance
L_{g}	gun inductance
L_i	inductance associated with the ith segment
m	mass of the plasma sheath, $m = \sum_{i=1}^{N} m_i$
m_i	mass of the ith segment
N	number of conical segments
v_i	velocity of the ith segment
p_i	momentum of the ith segment
Q	stored charge
Q_0	initial stored charge
R_0	initial effective resistance
r_1	anode radius
r_2	cathode radius
r_i	mean radius of the ith segment
R_{ext}	external resistance
R_{g}	effective incubation resistance
z	axial position along the gun
μ_0	vacuum magnetic permeability
ρ_0	density of the stagnant gas
θ_i	inclination angle of the ith segment

1. Introduction

One of the most efficient small fusion devices is the plasma accelerator gun (plasma focus [1–3]). The Mather-type gun consists of a pair of coaxial cylindrical electrodes located in a chamber filled with gas at low pressure (0.5–10 mbar). One end of the gun is closed, whereas the other end is open. In the closed end the electrodes are separated by a cylindrical coaxial insulator (see figure 1). When a capacitor bank charged at high voltage is connected to the system, an annular radial-current sheath is produced in the interelectrode space, over the insulator. The Lorentz force acting on the current accelerates the plasma towards the open end

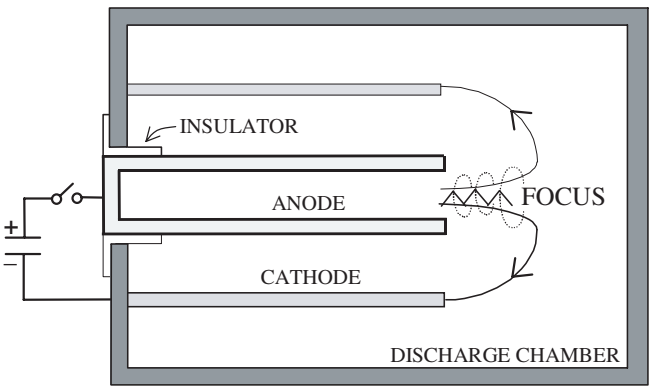

Figure 1. Diagram of the plasma focus device.

of the electrodes, where the sheath implodes into a hot dense focus in the axis. When deuterium or deuterium–tritium mixtures are used, fusion reactions occur during the focus, generating an intense pulse of neutrons, protons, ions, electrons and photons. Photonic emission covers a wide broadband espectra ranging from visible light up to hard x-rays. Apart from allowing basic plasma research, these machines form the core of a number of industrial applications ranging from tailored soft x-ray sources [4] and soft x-ray microlithography [5], to hard x-ray introspective imaging of metallic pieces [6] and neutronic detection of hydrogenated substances by neutron scattering [7].

The computer aided optimization of plasma focus devices, either as fusion machines and/or particle accelerator or as an x-ray source, requires the calculation of the sheath movement and the sensibility of the process to geometrical and operational parameters. This calculation involves the tracking of the ionizing shock accelerated to hypersonic velocities. During the displacement, the shape of the current sheath changes, inducing, in turn, variations on the boundary conditions, the forces and on the dissipation rates. There are several papers published in the literature on the plasma focus sheath modelling. For instance, a two-dimensional model of the current sheath coupled with the external circuit can be found in [8]. This model has the advantage of being analytical, but certain simplifications were made on the mechanical equation of the sheath for the sake of obtaining analytical results. In other cases, a complete numerical solution is obtained, but considering a one-dimensional, plane, current sheath [9, 10]. Detailed two-dimensional two-fluid magnetohydrodynamical models were also developed in Eulerian coordinates [11, 12], but intensive calculations are required to solve the corresponding numerical code.

In this work, an experimental study of the initial acceleration of the current sheath in a plasma focus is presented and compared with a computational model of the movement and shaping of a two-dimensional plasma sheath. Focalization times are also measured and compared with the numerical results. The main aim of this work is to present and develop a two-dimensional model keeping it as simple as possible whilst capable of reproducing experimental data.

2. Experimental study

The experiments were conducted on a small plasma focus device operated with deuterium driven by a capacitor bank having 4.7 kJ of stored energy connected to the electrodes through a switch (spark-gap). The parameters of the experiment are shown in table 1. A Rogowski coil and a magnetic probe were used to measure the focusing time and the plasma sheath evolution during the first stages of the discharge, respectively.

Table 1. Parameters of the experiment.

Parameter	Value
Anode length	120 mm
Cathode length	120 mm
Insulator length	35 mm
Insulator thickness	5 mm
Anode radius	18 mm
Cathode radius	36 mm
Initial voltage	30 kV
Capacity	10.5 μF
External inductance	42.6 nH

Figure 2 shows the signal measured with a Rogowski coil (output proportional to the time derivative of the current). The burst that is observed at 1 μs corresponds to the inductance perturbation during the focus. Figure 3 shows the measured dependence of the arrival time to the focus with the filling pressure. As expected, the sheath arrives later for higher pressures due to the larger mass accumulation.

A miniaturized glass-encased magnetic probe was located at different radial positions respect to the insulator surface (figure 4). Figure 5 shows the signal recorded by the probe when its sensing coil was placed at 3.00 ± 0.05 mm from the insulator during a discharge at a filling pressure of 1 mbar. The peak of the signal can be used to define the moment when the current sheath passes over the radial position of the probe's sensing coil. These signals were recorded at several radial distances at four different filling pressures (0.5, 1, 3 and 5 mbar). The spatial resolution of the probe, related to both, the size of its encasing body and to the relative position of its sensing coil respect to the probe's tip, is 3.9 mm. This means that an infinitely thin plasma sheath will produce a $\sim$4 mm wide peaked signal on the probe output [13]. The peak on the probe signal will approximately coincide (within a sensing coil radius, which is 1 mm) with the passing of the plasma sheath through the centre of the sensing coil.

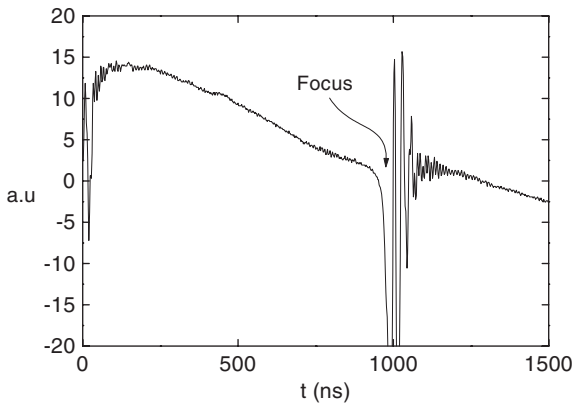

Figure 2. Rogowski signal (1 mbar).

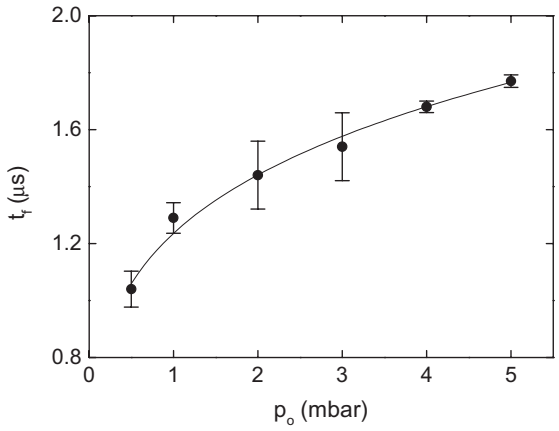

Figure 3. Dependence of the arrival time to the focus on the filling pressure.

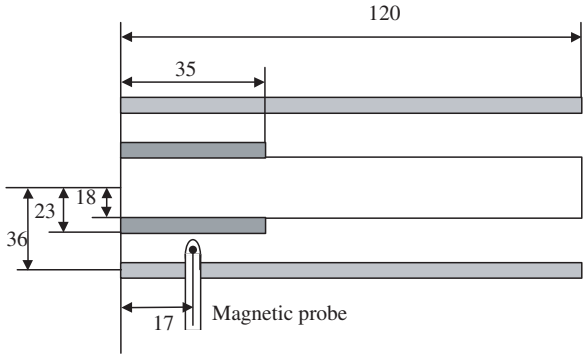

Figure 4. Diagram of the experimental apparatus showing the location of the magnetic probe (dimensions are in millimetres).

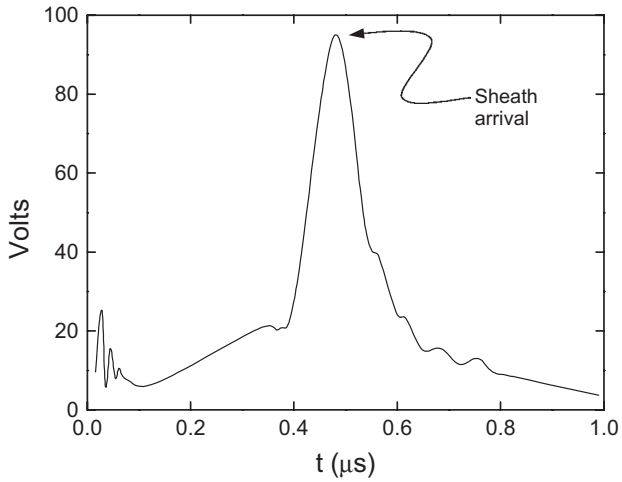

Figure 5. Probe signal when the sensing coil is placed at 3.00 ± 0.05 mm from the insulator surface. Filling pressure: 1 mbar.

Figure 6 shows the measured arrival time obtained from the probe signals. The vertical axis corresponds to the probe's tip position respect to the external radius of the insulator. The distance from the sensing coil to the probe's tip is 2.60 ± 0.05 mm. The statistical deviation of the measured arrival time is 25 ns. It can be observed that there is an incubation period, during which no sheath movement is detected, which is longer for higher pressures. Another observation is that the radial velocity of the sheath decreases with the pressure.

3. Numerical model

After closing the switch, it is considered that a gas discharge starts in the gap between the electrodes forming an umbrella-like plasma layer over the insulator surface. The azimuthal magnetic field located in the toroidal volume enclosed by the current produces a $\vec{J} \times \vec{B}$ force that acts as a piston driving the sheath toward the open end of the electrodes. The run-down of the current sheath is a sweeping supersonic shock that propagates collecting the gas particles ahead of the front (snowplow scenario [14]). On its arrival at the open end (some microseconds

after triggering), the magnetic field accelerates the plasma towards the axis. Finally, the sheath clashes on the axis in the form of a small dense plasma cylinder (focus). The complete process lasts for about 1 μs, depending on the filling pressure, whereas the lifetime of the focus is about 300 ns.

The current sheath was modelled by means of a class of geometric objects (conical segments) with attributes representing the mechanical and thermodynamic state of the plasma in the corresponding region: mass, position, velocity, acceleration, density and internal energy. Each plasma segment moves normal to its surface (figure 7) accelerated by the Lorentz force according to:

$$\frac{\mathrm{d}p_i}{\mathrm{d}t} = \frac{\mu_0}{4\pi}\frac{l_i}{r_i}I^2 \tag{1}$$

During the displacement, the segments accumulate the gas mass swept by the shock, that is:

$$\frac{\mathrm{d}m_i}{\mathrm{d}t} = \rho_0 A_i v_i \tag{2}$$

The segments beyond the cathode are allowed to abandon the current sheath because usually the external electrode is an arrangement of metallic bars (see figure 8).

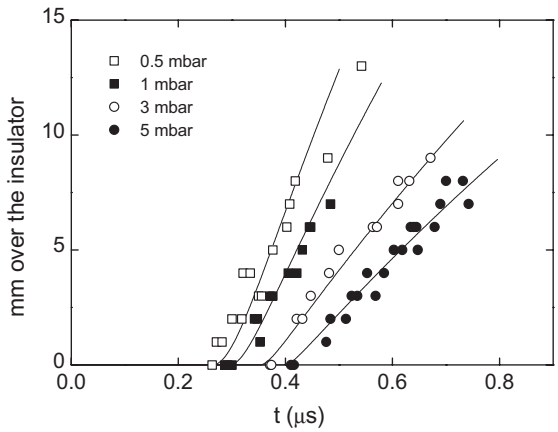

Figure 6. Movement of the current sheath during the first stages of the discharge.

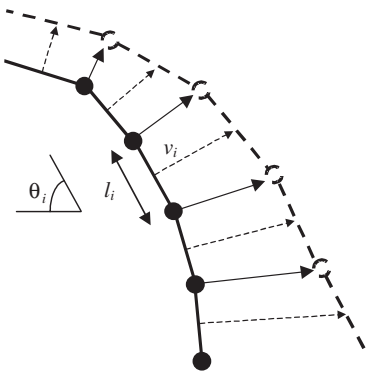

Figure 7. Model of the movement of the plasma sheath.

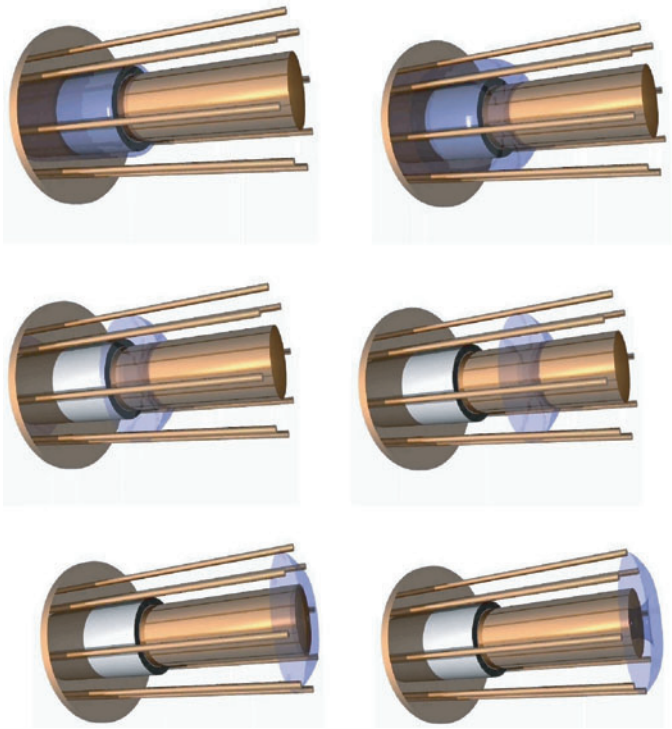

Figure 8. Images of the simulation.

3.1. Sheath tracking and shaping

The following algorithm was implemented to ensure that the shock-front displacement responds to the conservation equations and that the conical segments move normal to their respective surface:

(1) Calculate the displacement that each segment should perform according to the conservation equations (dashed arrows in figure 7).
(2) Move the nodes (junctions between segments) according to a vector calculated as the mean displacement of the corresponding adjacent segments.

Once this algorithm is applied, the lengths of the segments change. According to their attributes some segments grow faster than others, leading to representations with segments having much different length between them. This effect can produce geometric local instabilities. In order to avoid this problem, after each time step the sheath is reshaped with segments of equal length, keeping constant the number of nodes per unit length along the sheath. The procedure is the following:

(1) Calculate the length l_i^{new} , which each segment should have in order to keep constant the number of nodes per unit length.
(2) Construct a new representation of the sheath starting from the inner boundary, with segments having the new lengths, taking the mass, momentum and energy of the replaced old segments proportionally to the corresponding length.

3.2. Equations of the electrical circuit

From the electrical point of view, the plasma gun is represented as a time dependent inductance coupled with a RCL series circuit. The corresponding equations are:

$$\frac{\mathrm{d}}{\mathrm{d}t}[(L_{\mathrm{ext}} + L_{\mathrm{g}})I] + (R_{\mathrm{ext}} + R_{\mathrm{g}})I - \frac{Q}{C} = 0 \tag{3}$$

$$-\frac{\mathrm{d}Q}{\mathrm{d}t} = I \tag{4}$$

where L_{ext} and R_{ext} are the stray inductance and resistance, respectively, associated with the electrical connection between the capacitor bank and the electrodes.

The inductance of the gun corresponds to a coaxial geometry of variable radius. The contribution of each conical segment is calculated as:

$$L_i = \frac{\mu_0}{2\pi} l_i \cos\theta_i \ln\left(\frac{r_{\mathrm{Max}}}{r_{\mathrm{Min}}}\right) \tag{5}$$

being

$$r_{\mathrm{Max}} = \begin{cases} r_i & r_1 \leqslant r_i < r_2 \\ r_1 & r_i < r_1 \end{cases} \tag{6}$$

$$r_{\mathrm{Min}} = \begin{cases} r_1 & r_1 \leqslant r_i < r_2 \\ r_i & r_i < r_1 \end{cases} \tag{7}$$

The total inductance of the gun is the summation of all the elemental conical contributions plus the rectilinear part of the gun, located between the closed end of the electrodes (axial position $z = 0$) and the conical segment touching the external electrode (radial position = r_2, axial position = z_N):

$$L_{\mathrm{g}} = \sum_{i=1}^{N} L_i + \frac{\mu_0}{2\pi} z_N \ln\left(\frac{r_2}{r_1}\right) \tag{8}$$

The initial conditions for solving equations (1)–(4) are

$$m_i|_{t=0} = 10^{-20}\,\mathrm{kg}, \qquad v_i|_{t=0} = 0, \qquad Q|_{t=0} = Q_0, \qquad \left.\frac{\mathrm{d}Q}{\mathrm{d}t}\right|_{t=0} = 0. \tag{9}$$

3.3. Breakdown modelling

In order to take into account the initial stages, it is necessary to describe mathematically the breakdown process, because it introduces certain delays that play a significant role in the arrival timing. Actually, the breakdown is a quite complex phenomenon that involves several physical processes occurring during the circuit closure [15, 16]. In discharge devices such as the one used in the experiments presented in this paper, there are two points of gas dielectric breakdown: the spark-gap switch and the layer surrounding the insulator in the coaxial gun.

The ionization process occurring over the annular insulator at the closed end of the gun can be modelled imposing an incubation period before the plasma sheath is completely formed and ready to move forward [15]. A simple model of this process is an effective dissipative resistance, simulating the accumulation of internal energy in the actual sheath at a rate proportional to the square of the current. The sheath starts moving when the internal energy reaches the threshold required to ionize 80% of the gas mass contained in an effective thin layer attached to the insulator. The electrical resistance of the partially ionized sheath is assumed to be:

$$R_{\mathrm{g}} = R_0\left(1 - \frac{e}{e_{\mathrm{I}}}\right) \tag{10}$$

and the specific internal energy of the layer, e, is calculated from:

$$\frac{\mathrm{d}(em)}{\mathrm{d}t} = R_{\mathrm{g}} I^2 \tag{11}$$

with $em_i|_{t=0} = 0$.

The spark-gap was modelled as a constant resistance, R_{ext}, acting during a switching period τ_{sg}.

3.4. Object-oriented computational implementation

The system of equations (1)–(4) with definitions (5)–(8) and the initial conditions (9), together with the simplified breakdown model (10) and (11) and the above-mentioned tracking and shaping algorithm, can be implemented and solved with any ordinary differential equations solver, such as the Runge–Kutta method [17], to get the current sheath position, velocity and shape as function of time together with the circulating current and energy dissipation. Alternatively, the same results can be obtained implementing an object-oriented algorithm for the sake of computational efficiency. In this work we decided to instrument the second approach as follows.

A simulator was designed and implemented following the object-oriented paradigm, creating a class hierarchy that reflects the device composition. The application was instantiated in a framework based in the architecture Model-View by means of the implementation of the pattern Observer [18]. The architecture design was based in the separation of functionalities in four components. The Model component includes the classes representing physical elements. The SimulationManager component manages the interaction between the Model objects. The Equations component contains TEquation classes representing the differential equations governing the behaviour of the objects of Model component. The Integrator component manages the numerical integration of the equations by means of a fourth order Runge–Kutta scheme.

The class TModel, defined in the Model component, implements a common interface that retrieves the state variables of the subclasses. A particular subclass of TModel is SimModel, which is the base class of any class described by a differential equation. The main SimModel subclasses are ExternalCircuit, PlasmaGun and PlasmaSegment, representing the corresponding elements of the plasma focus device. The geometric attributes of the device are introduced as attributes of ExternalElectrode, InnerElectrode and Insulator, which are subclasses of TModel.

In every time step, SimulatorManager passes all the SimModel objects (i.e. objects whose behaviour is represented by differential equations), and the corresponding TEquation objects, to the Integrator, which solves in parallel the set of differential equations over the time step.

4. Results and discussion

The model was used to simulate the plasma-shock run-down along the coaxial tube described in table 1, using a node density of 10 nodes per centimetre. Figure 8 shows a three-dimensional sequence visualization of the simulated evolution of the plasma sheath.

Figure 6 shows the curves (continuous traces) corresponding to the calculated radial movement of the current sheath for each deuterium pressure. The curve in figure 3 represents the predicted arrival times to the focus. It can be seen that the model follows the experimental trends very well.

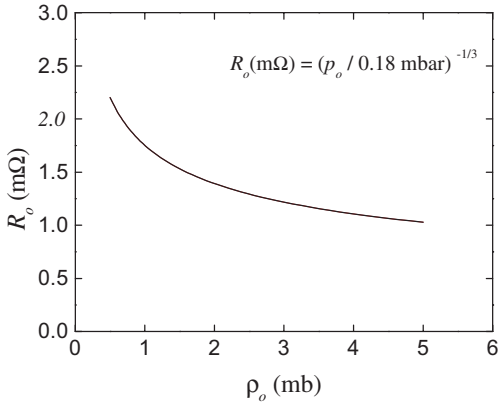

Figure 9. Effective initial resistance of the plasma sheath (equation (10)).

The effective parameters of the spark-gap are:

$$R_{\text{ext}} = 0.26\,\Omega$$
$$\tau_{\text{sg}} = 7\,\text{ns}$$

The pressure dependence of the effective resistance, R_0, of the incipient plasma layer is shown in figure 9. The results are insensitive to the initial mass of the layer, within a reasonable range of values ($m \approx 10^{-20}$–10^{-9} kg). It was found that R_0 decreases monotonically with the filling pressure, which is acceptable taking into account that the density of electrons is higher for higher pressures [16, 19].

Although simplified models for each breakdown phase and the spark-gap are used, the presented set of equations plus the sheath tracking and shaping algorithm was proven to bring accurate enough results to reproduce experimental data taken during the first stages of the discharge, as well as the final ones.

5. Conclusion

A two-dimensional computer simulation model of the movement and shaping of the current sheath in a plasma focus was presented and compared with experimental results. The tracking of the current sheath during the acceleration requires the application of a reshaping technique to avoid numerical instabilities. The dielectric breakdown was described by means of an effective model of dissipation during the plasma layer formation.

The theory was able to represent very well the experimental trends during the radial expansion of the plasma near the insulator as well as the focusing time, and can be used to analyse the movement and shaping of magnetically driven shocks in other geometries or gases. However, care should be taken regarding the values of the effective parameters, because they can differ from case to case. Further studies in this direction can provide a convenient set of values that covers a wide range of situations.

Acknowledgments

This work was supported by PLADEMA and by a research grant from UBA (X074). The authors also acknowledge Dr R Vieytes for the critical reading of the manuscript.

References

[1] Mather J W 1964 Investigation of the high-energy acceleration mode in the coaxial gun *Phys. Fluids* **7** 5–28

[2] Mather J W 1971 Dense plasma focus *Methods of Experimental Physics* vol 9B, ed H Lovberg and H R Griem (New York: Academic) pp 187–249

[3] Filippov N V and Filippova T I 1965 *Proc. 2nd IAEA Conf. on Plasma Physics and Controlled Nuclear Fusion Research* (Culham) vol 2 pp 405–16

[4] Zakaullah M, Alamgir K, Shafiq M, Sharif M, Waheed A and Murtaza G 2000 Low-energy plasma focus as a tailored x-ray source *J. Fusion Energy* **19** 143–57

[5] Lee S, Lee P, Zhang G, Feng X, Gribkov V, Liu M, Serban A and Wong T K S 1998 High rep rate high performance plasma focus as a powerful radiation source *IEEE Trans. Plasma Sci.* **26** 1119–26

[6] Moreno C, Clausse A, Martínez J F, Llovera R and Tartaglione A 2001 Ultrafast x-ray introspective imaging of metallic objects using a plasma focus *Nukleonika* **46** (Suppl. 1) S33–4

[7] Moreno C, Clausse A, Martínez J, Llovera R, Tartaglione A, Vénere M, Barbuzza R and del Fresno M 2001 Using a 4.7 kJ plasma focus for introspective imaging of metallic objects and for neutronic detection of water *Proc. 9th Latin American Workshop on Plasma Physics* ed H Cuaqui and M Favre *AIP Conf. Proc.* **563** 300–5

[8] Gratton F and Vargas M 1983 Two-dimensional electromechanical model of the plasma focus *Energy Storage, Compression, and Switching* vol 2, ed V Nardi *et al* (New York: Plenum) pp 353–86

[9] Lee S 1990 Technology of a small plasma focus incorporating some experiences with the UNU/ICTP PFF *Small Plasma Physics Experiments* vol II, ed S Lee and P H Sakanaka (Singapore: World Scientific) pp 113–69

[10] Mathuthu M, Zengeni T G and Gholap A V 1997 The three-phase theory for plasma focus devices *IEEE Trans Plasma Sci.* **25** 1382–8

[11] Potter D E 1971 Numerical studies of the plasma focus *Phys. Fluids* **14** 1911–24

[12] Maxon S and Eddleman J 1978 Two-dimensional magnetohydrodynamic calculation of the plasma focus *Phys. Fluids* **21** 1856–65

[13] Bruzzone H, Moreno C and Kelly H 1991 Measurements of current sheets in plasmas with a finite-sized magnetic probe *Meas. Sci. Technol.* **2** 1195–200

[14] Rosembluth M and Garwin R 1954 *Technical Report* Los Alamos Scientific Laboratory, LA-1850

[15] Bruzzone H and Vieytes R 1993 The initial phase in plasma focus devices *Plasma Phys. Control. Fusion* **35** 1745–54

[16] Korolev Yu D and Mesyats G A 1998 *Physics of Pulsed Breakdown in Gases* URO-PRESS

[17] Press W H, Flannery B P, Teukolsky S A and Vetterling W T 1988 *Numerical Recipes in C: The Art of Scientific Computing* (New York: Cambridge University Press)

[18] Meyer B 1977 *Object-Oriented Software Construction* 2nd edn (Englewood Cliffs, NJ: Prentice-Hall)

[19] Meek J M and Craggs J D (ed) 1978 *Electrical Breakdown in Gases* (New York: Wiley)